

Sputter gas pressure effects on the properties of Sm-Co thin films deposited from a single target.

T. G. A. Verhagen, D. B. Boltje, J. M. van Ruitenbeek and J. Aarts^{1, a)}

Kamerlingh Onnes Laboratorium, Universiteit Leiden, PO Box 9504, 2300 RA Leiden, The Netherlands

(Dated: 24 March 2024)

We grow epitaxial Sm-Co thin films by sputter deposition from an alloy target with a nominal SmCo_5 composition on Cr(100)-buffered MgO(100) single-crystal substrates. By varying the Ar gas pressure, we can change the composition of the film from a SmCo_5 -like to a Sm_2Co_7 -like phase. The composition, crystal structure, morphology and magnetic properties of these films have been determined using Rutherford Backscattering, X-ray diffraction and magnetization measurements. We find that the various properties are sensitive to the sputter background pressure in different ways. In particular, the lattice parameter changes in a continuous way, the coercive fields vary continuously with a maximum value of 3.3 T, but the saturation magnetization peaks when the lattice parameter is close to that of Sm_2Co_7 . Moreover, we find that the Sm content of the films is higher than expected from the expected stoichiometry.

PACS numbers: 75.50.Vv, 75.50.Ww, 75.70.Ak, 76.30.Fc

Keywords: SmCo_5 , Sm_2Co_7 , sputtering

I. INTRODUCTION

Modern permanent magnetic materials, like SmCo_5 and NdFe_{14}B , are based on intermetallic compounds of rare-earth and 3d transition metals. Sm-Co intermetallics are hard magnetic materials with a high coercive field and a high uniaxial magnetocrystalline anisotropy, where the easy axis is aligned along the crystallographic c -axis. Since the 1970s/1980s many groups investigated the properties of Sm-Co crystals and thin films. The control of the composition and the crystallographic texture are the key parameters to obtain thin films with the desired hard magnetic properties. These properties are interesting from both a technical and a fundamental point of view. The further miniaturization of magnetic microelectromechanical systems (MEMS)¹ requires the control of such films. But also the combination between a hard magnet like SmCo_5 with soft magnets² or superconductors³ is an unexplored area that can lead to interesting and useful magnetic configurations.

In the last years, recipes have been developed to grow films with the desired hard magnetic properties. One way to obtain them is to grow epitaxial thin films. Epitaxial growth can be obtained by using MgO(100), MgO(110) and Si(100) single crystals, commonly in combination with a chromium buffer layer. Growing Sm-Co films on the four-fold symmetric MgO(100) substrates results in the epitaxial relation $\text{Sm-Co}(11-20)[0001]//\text{Cr}(001)[110]//\text{MgO}(001)[100]$, where in the film the Sm-Co grains are equally distributed along the two in-plane directions. Sm-Co films can also be deposited on a glass substrate. Growing on glass results in very small crystallites in a disordered structure, and

yields large coercive fields⁴.

Most groups grow thin Sm-Co films using pulsed-laser deposition (PLD)⁵ or sputter deposition⁶ from single elemental targets Sm and Co. By tuning the sputter power of both sources or the pulse ratio by PLD, it is possible to grow compositions in the desired range. Also the influence of the substrate temperature has been studied, for obtaining epitaxial films. The effect on the film growth of the sputter background pressure is often not taken into account. Still, the sputter pressure plays an important role in the growth kinetics and one recent study showed that changes in the stoichiometry and magnetic properties occur when varying the pressure⁷. One of the underlying problems is the complexity of the Sm-Co phase diagram⁸ in which, on the Co-rich side, the compounds $\text{Sm}_2\text{Co}_{17}$ (11 % Sm), SmCo_5 (17 % Sm), $\text{Sm}_5\text{Co}_{19}$ (21 % Sm) and Sm_2Co_7 (22 % Sm) all exist; with the note that SmCo_5 actually is a metastable compound. The connection between composition and magnetic properties is therefore not trivial. Fortunately, high coercive fields can be found over a range of compositions and a number of studies has focused on this particular aspect.

In this paper, we show that by varying the argon pressure, we are able to grow SmCo_5 -like and Sm_2Co_7 -like phases from an alloy target, with good crystallographic texture, coercive field and saturation magnetization. The properties of the grown films are shown to be very sensitive to the sputter pressure used.

II. EXPERIMENT

The Sm-Co films were deposited in a UHV chamber (base pressure $1 \cdot 10^{-9}$ mbar) using DC magnetron sputter deposition with argon as plasma from a commercially obtained alloy target with a nominal composition of SmCo_5 (3N). A rotating sample holder was used. The de-

^{a)}Electronic mail: aarts@physics.leidenuniv.nl

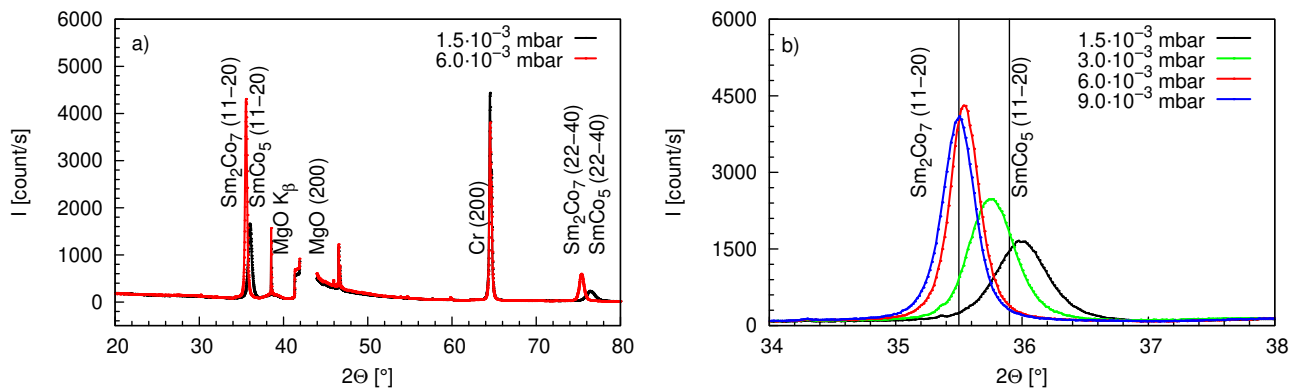


FIG. 1. a) θ - 2θ XRD scans of Sm-Co films grown from an Sm-Co alloy target on a Cr/MgO(100) substrate with two different sputter gas pressures as indicated. b) shows the region around the Sm-Co(11-20) peak, where the two vertical lines indicate the reflection of bulk crystalline Sm_2Co_7 (left) and SmCo_5 (right). Four samples are shown, grown at (from right to left), $1.5 \cdot 10^{-3}$ (black), $3.0 \cdot 10^{-3}$ (green), $6.0 \cdot 10^{-3}$ (red) and $9.0 \cdot 10^{-3}$ mbar (blue).

position rate was measured by X-ray reflectivity (XRR) using Cu-K α radiation.

Films were deposited on 500 μm thick MgO(100) single crystal substrates on which a 100 nm thick Cr buffer layer was first deposited at 250°C in an Ar pressure of $1.5 \cdot 10^{-3}$ mbar. All Sm-Co films were approximately 100 nm thick and were grown at 450°C with an Ar pressure varying between $1.5 \cdot 10^{-3}$ mbar and $12.5 \cdot 10^{-3}$ mbar. Afterwards, a 10 nm thick Cr layer was deposited at 450°C as a protection layer.

The actual film composition and thickness were determined using Rutherford Backscattering (RBS). The structural quality of the film was measured with θ - 2θ X-ray diffractometry (XRD) using Cu-K α radiation, where the MgO substrate peak was measured as a reference for the angle, by using an extra Cu-absorber to decrease the intensity. The morphology of the films was characterized by Atomic Force Microscopy (AFM) in tapping mode. Magnetization measurements were performed in a SQUID-based magnetometer (MPMS 5S from Quantum Design) in fields up to 5 T. For the magnetization measurements, the substrates were cut in pieces of approximately $10 \times 4 \text{ mm}^2$. As a reference, an MgO(100) substrate was measured, and also an MgO(100) substrate with a 100 nm Cr film protected with 30 nm Cu. Electron paramagnetic resonance (EPR) spectra were measured at room temperature using a Bruker EMX plus X-band spectrometer in a TE₀₁₁ cavity with 100 kHz modulation frequency and 1 G modulation amplitude.

III. RESULTS

Figure 1(a) shows the XRD scans of films grown at $1.5 \cdot 10^{-3}$ mbar (SmCo_5 -like) and $6.0 \cdot 10^{-3}$ mbar (Sm_2Co_7 -like) respectively. The observed peaks are labeled as reflections of Sm-Co, MgO and Cr. Due to the thickness and high crystallinity, also the K_β peak

of the MgO substrate is visible. In Figure 1(b) the region around the Sm-Co(11-20) peak is shown, for films grown with a sputter pressure of 1.5, 3.0, 6.0 and $9.0 \cdot 10^{-3}$ mbar. Clearly visible is that, with decreasing pressure, the peaks shift to a higher angle. The measured lattice constant, determined from the Sm-Co(22-40) peak, and the Sm content are plotted in Figure 2 as a function of the sputter pressure. For films grown at a pressure above $6.0 \cdot 10^{-3}$ mbar, the lattice parameter of the Sm-Co film is almost that of bulk Sm_2Co_7 (0.5040 nm). Decreasing the pressure from $6.0 \cdot 10^{-3}$ mbar shows a decreasing lattice parameter, and at the lowest pressure the lattice constant of the Sm-Co film just reaches the SmCo_5 bulk value (0.4982 nm). With respect to the Sm concentration, we consistently find a somewhat higher number than the stoichiometric Sm-Co phases would yield. Above $6.0 \cdot 10^{-3}$ mbar, the Sm concentration is around 25 - 27 % (compared to 22 % for Sm_2Co_7). Below $6.0 \cdot 10^{-3}$ mbar the Sm content gradually decreases to 21 % (compared to 17 % for SmCo_5).

Figure 3(a)-(d) show the morphology of the Sm-Co films grown at 1.5, 3.0, 6.0 and $9.0 \cdot 10^{-3}$ mbar, respectively. The films grown at a high sputter background pressures consists of rectangular grains with an average size of $70 \times 250 \text{ nm}^2$. Statistical analysis over an area of $1 \times 1 \mu\text{m}^2$ on the Sm-Co film grown at $6 \cdot 10^{-3}$ mbar indicates an average surface roughness of 8.1 nm and a peak to peak value of 57 nm. When decreasing the pressure below $6 \cdot 10^{-3}$ mbar, the shape of the grains slowly transforms from rectangular to square-like. Sm-Co films grown at $1.5 \cdot 10^{-3}$ mbar consist of square grains with an average size of $75 \times 75 \text{ nm}^2$. Statistical analysis over an area of $1 \times 1 \mu\text{m}^2$ on the Sm-Co film grown at $1.5 \cdot 10^{-3}$ mbar indicates an average surface roughness of 9.6 nm and a peak to peak value 55 nm.

In Figure 4 the magnetization measurements are shown, taken at room temperature. The magnetization was calculated by dividing the measured magnetic

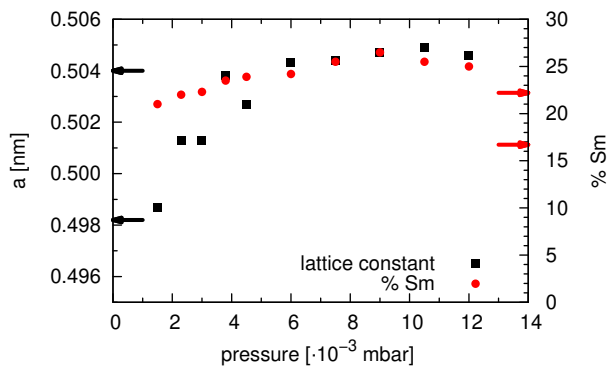


FIG. 2. The lattice constant and the Sm concentration of the Sm in Sm-Co films as a function of the sputter background pressure, where the black (\leftarrow) and red (\rightarrow) arrows indicate the lattice constant and Sm concentration of bulk SmCo_5 and Sm_2Co_7 . Clearly visible is the change of the lattice parameter a from the Sm_2Co_7 phase ($a=0.5040$ nm) to the SmCo_5 phase ($a=0.4982$ nm).

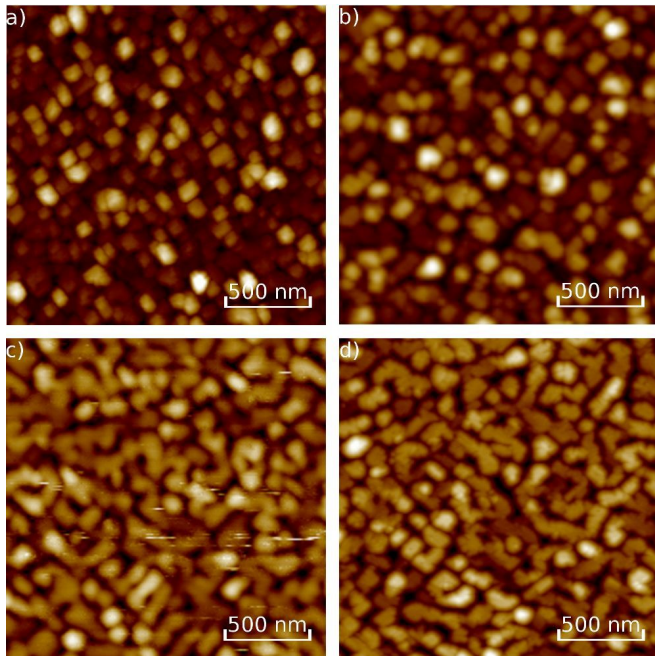


FIG. 3. Morphology of the Sm-Co film grown at a) $1.5 \cdot 10^{-3}$, b) $3 \cdot 10^{-3}$, c) $6 \cdot 10^{-3}$ and d) $9.0 \cdot 10^{-3}$ mbar measured with atomic force microscopy.

moment by the measured volume of the Sm-Co films (typically $10 \text{ mm} \times 4 \text{ mm} \times 100 \text{ nm}$). All samples show hysteretic behavior with a square-like loop and a large coercivity, of the order of 3 T, but also a substantial diamagnetic contribution. Separate measurements on an $\text{MgO}(100)$ substrate and an $\text{MgO}(100)/\text{Cr}(100 \text{ nm})/\text{Cu}(30 \text{ nm})$ film show that, at room temperature, the magnetic susceptibility χ of MgO for substrates from different batches varied and the samples measured had a magnetic susceptibility of -2.4 and $-3.5 \cdot 10^{-7}$ emu/g.

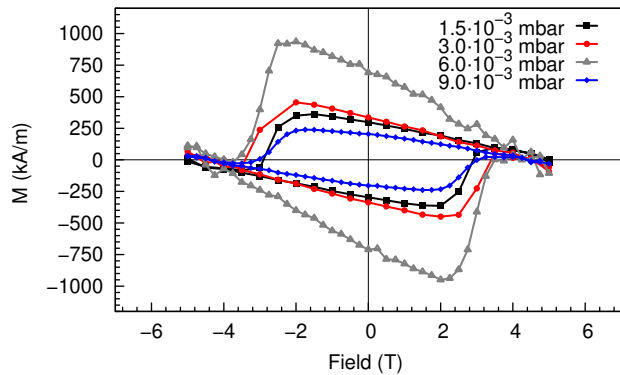


FIG. 4. Uncorrected magnetic hysteresis of the Sm-Co film on a $\text{Cr}/\text{MgO}(100)$ substrate grown with different sputter gas pressures as indicated at 300 K.

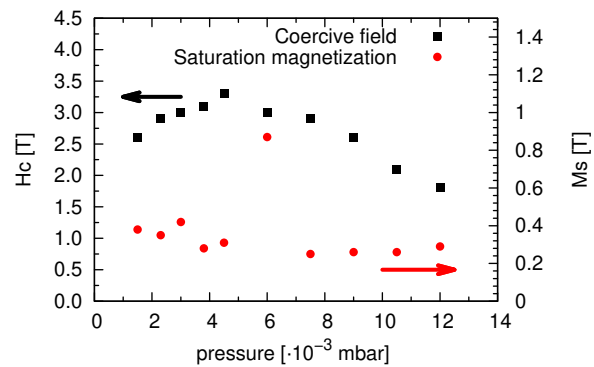


FIG. 5. The coercive field and the saturation magnetization of the Sm-Co films as a function of the sputter background pressure.

These values are in agreement with $\chi = -5.1 \cdot 10^{-7}$ emu/g for a single-crystal MgO^9 .

For the films grown at 1.5 , 3.0 and $9.0 \cdot 10^{-3}$ mbar, the coercive field H_c is approximately 2.5 T and the saturation magnetization M_s is approximately 0.4 T. The film grown at $6.0 \cdot 10^{-3}$ mbar has a slightly higher coercive field of 3.0 T and a significantly larger saturation magnetization of 0.87 T. Both H_c and M_s as a function of sputter pressure are given in Figure 5. Again we find clear trends: with increasing pressure up to $6 \cdot 10^{-3}$ mbar H_c slowly increases from 2.6 T to 3.3 T, but above $6 \cdot 10^{-3}$ mbar a rapid decrease sets in, down to 1.8 T at $12 \cdot 10^{-3}$ mbar. The saturation magnetization is 0.3-0.4 T in the whole pressure range, but clearly visible is the much higher saturation magnetization of the film grown at $6.0 \cdot 10^{-3}$ mbar. To characterize the magnetic texture, the ratio of the remnance of the in-plane and out-of-plane magnetizations was determined for the films grown at 1.5 and $6.0 \cdot 10^{-3}$ mbar (not shown). These data show that both films have a preferred in-plane texture.

We also investigated the low temperature behavior of

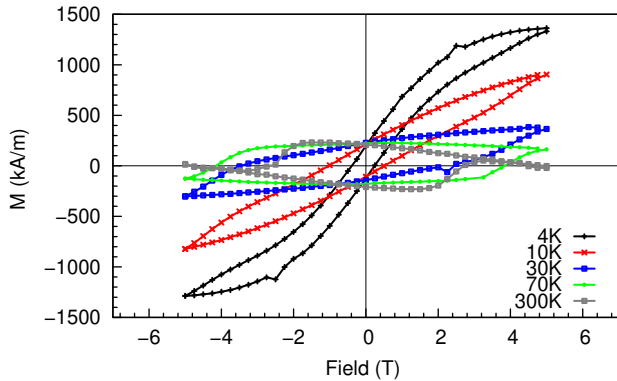


FIG. 6. a) Uncorrected magnetic hysteresis of the Sm-Co film grown at $10.5 \cdot 10^{-3}$ mbar as a function of temperature. For the 10 K and 4 K loop, the 5 T magnet of the magnetometer is not strong enough to reach the coercive field of the Sm-Co film and the contribution of the MgO substrate increases significantly.

the Sm-Co films. In Figure 6, the uncorrected magnetization hysteresis loops for a Sm-Co film grown at $10.5 \cdot 10^{-3}$ mbar are shown as a function of temperature. For temperatures down to 30 K, the coercive field and the saturation magnetization increase slowly. Also, the diamagnetic contribution of the substrate becomes smaller. When going to even lower temperatures, the hysteresis loop shows a clear paramagnetic behavior. Figure 7(a) shows the uncorrected hysteresis loop for two MgO substrates from different batches at 4 K. Also here the low temperature magnetization measurements show a clear paramagnetic behavior. Electron paramagnetic resonance (EPR) measurements were done to identify the paramagnetic impurities. Figure 7(b) shows the room temperature EPR measurements of a MgO substrate. Clearly visible are the resonance lines of Cr^{3+} , V^{2+} and Mn^{2+} impurities¹⁰. In Figure 8, the uncorrected and corrected magnetization hysteresis loops at 4.2 K for a Sm-Co film grown at $2.3 \cdot 10^{-3}$ mbar are shown. Clearly visible is that the uncorrected loop is a minor loop, where the remanent magnetization for both the positive and negative field sweep has the same high and positive value. The magnetization hysteresis loop is corrected by subtracting the magnetization of the impurities. The corrected hysteresis loop is almost field independent, showing that the coercive field is larger than 5 T.

IV. DISCUSSION

Summarizing the experimental findings, we see that with increasing sputter pressure, the lattice parameters and the values for H_c increase until the pressure of $6.0 \cdot 10^{-3}$ mbar is reached, where the lattice parameter corresponds to the Sm_2Co_7 alloy. At this pressure M_s increases sharply. Increasing the pressure further,

M_s comes down again, while H_c now starts to decrease. In the whole range, we find the Sm content of the films higher than expected from the stoichiometric ratios of the line compounds. Apparently, the sputter process does not result in a well-defined composition. In particular, the films are not a mixture of the SmCo_5 and Sm_2Co_7 compounds, which would result in two lines with different weight in the x-ray data. Rather, the films consist of one main composition which is able to incorporate a varying amount of Co-atoms, probably in a complex with the detected surplus of Sm. Cross sectional transmission electron microscope data¹¹ have shown that when the Sm-Co film is not grown under the optimal conditions, different epitaxial growth modes exist. The film does not grow with a full crystalline structure and amorphous areas are formed where the remaining material is stored.

The surface morphology in Figure 3 shows that the grain size and grain shape changes when the sputter pressure is changed. At high pressures, relatively large rectangular grains are grown. When reducing the pressure, the grains become smaller and more square-like. We surmise this is due to the change in average energy of the atoms bombarding the substrate: at low pressure, this energy is higher and as a result, more defects are created during the growth of the first Sm-Co layers. When the number of defects becomes larger, also the number of preferred nucleation sites increases. The increase in the number of nucleation sites results in a reduced grain size and a more rough surface. Magnetically, the picture is somewhat complicated by the paramagnetic behavior of the MgO substrates, which is due to transition metal impurities, in particular Mn, V, and Cr. Their amount varies from batch to batch. The low temperature magnetic hysteresis shows a clear paramagnetic behavior superimposed on it, so we assume that the magnetization M_{imp} of these impurities can be described by the Brillouin function

$$M_{\text{imp}} = NgJ\mu_B \frac{2J+1}{2J} \coth\left(\frac{2J+1}{2J} \frac{gJ\mu_B JB}{k_b T}\right) - NgJ\mu_B \frac{1}{2J} \coth\left(\frac{1}{2J} \frac{gJ\mu_B JB}{k_b T}\right) \quad (1)$$

with N the number of atoms, g the g-factor, μ_B the Bohr magneton, J the total angular momentum, k_B Boltzmann constant and T the temperature. The total magnetization for the three different impurities is then modelled as the sum of the magnetization of each type of impurities.

From fitting equation 1 to the low temperature magnetic hysteresis of a bare MgO substrate, we estimate that in the MgO substrates in Figure 7(a), the concentration of the impurities is in the range of 15-60 ppm¹². Another factor that influences the corrections made to the magnetization is the oxidation of the Cr capping layer, which induces an unknown extra magnetization.

Magnetically, the properties of the films grown at different sputter background pressures up to $6.0 \cdot 10^{-3}$ mbar are very similar. At 300 K, the films show a square

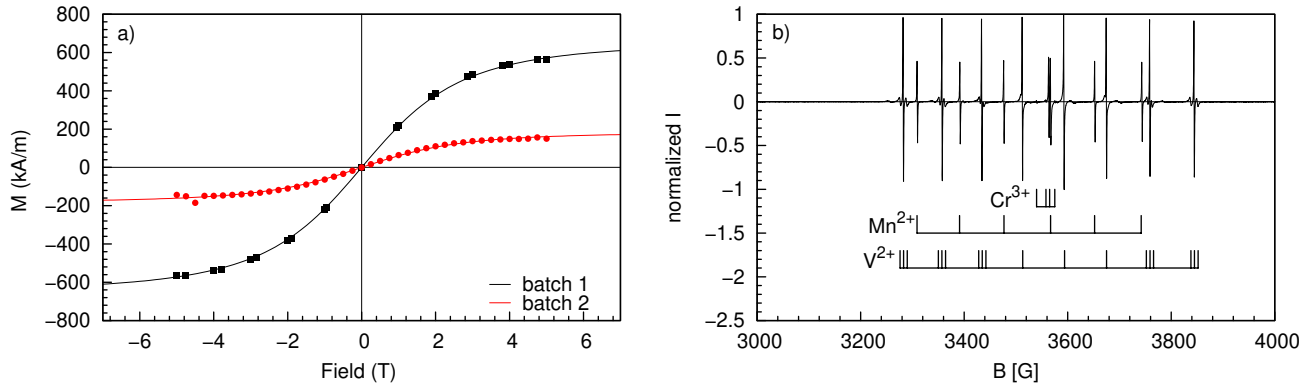


FIG. 7. a) Uncorrected magnetic hysteresis of two MgO substrates from different batches measured at 4 K. The spectra is fitted to a Brillouin function for the Cr^{3+} , Mn^{2+} and V^{2+} impurities. b) A typical room temperature epr spectrum is shown of a MgO single crystal substrate containing Cr^{3+} , Mn^{2+} and V^{2+} impurities.

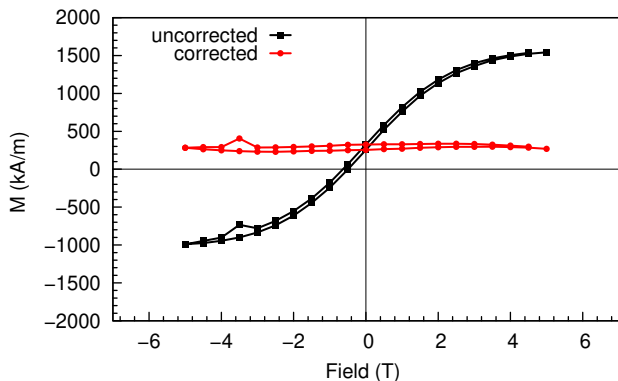


FIG. 8. Uncorrected and corrected magnetic hysteresis of the Sm-Co film grown at $2.3 \cdot 10^{-3}$ mbar at 4.2K.

hysteresis loop for the field applied in the plane of the sample, with a coercive fields of about 3 T and a saturation magnetization of 0.4 T. The films grown with a sputter background pressure above $6.0 \cdot 10^{-3}$ mbar show a decrease in coercive field, although the Sm concentration, lattice constant and saturation magnetization do not change significant with respect to the films grown at pressures below $6.0 \cdot 10^{-3}$ mbar. We attribute the change in coercive field to the larger grain size of the grown Sm-Co film. The grain size of thin Sm-Co films is hard to control, but the grain size of SmCo_5 powder can be controlled well by grinding and milling. In experiments with nanoparticles with a different size, it was found that the size has a significant influence on the coercive field and a optimum particle size is approximately 100-200 nm¹³.

Only the film grown at $6.0 \cdot 10^{-3}$ mbar shows a large saturation magnetization of 0.87 T. SmCo_5 and Sm_2Co_7 crystals have a saturation magnetization M_s of 1.05 and 1.29 T respectively. Due to the four-fold symmetry of the MgO(100) substrate, the saturation magnetization of the films will not have this values because part of the Sm-Co grains are aligned in-plane and the other grains

are aligned out-of-plane and do not contribute to the saturation magnetization when measured along the (100)- or (010)-axis.

The optimal sputter pressure to grow the SmCo_5 -like phase with a larger saturation magnetization might be lower than $1.5 \cdot 10^{-3}$ mbar, the lowest pressure at which we can grow films. This appears also from the fact that the Sm_2Co_7 -like phase can be grown over a large pressure window with a large coercive field but only at a very small pressure window gives a high saturation magnetization, as is shown in Figure 5.

At 4.2 K, the result is a little bit more complicated. When decreasing the temperature, the MgO substrate develops an induced moment. The Mn, Cr and V impurities add at low temperatures a paramagnetic contribution. The variation in the magnetic moment is quite large, as shown in Figure 7(a). Furthermore, Figure 8 shows clearly that the measured magnetic hysteresis loop is not the hysteresis loop itself, but a minor loop, since the coercive field is larger than the 5 T which can be reached in the magnetometer. When the contribution of the impurities in the MgO substrate is subtracted using equation 1, the Sm-Co film shows an almost constant magnetization.

A problem of growing Sm-Co films from an alloy target is, that the film composition is very sensitive to the target composition. We used a number of different commercially obtained targets which, according to the vendor, were fabricated from the same batch of alloy material. All targets had a slightly different Sm concentration. From Figure 2, it is clear that a small change in Sm concentration can change the magnetic and crystallographic properties a lot. The films grown with the other targets showed coercive fields between 1.0 and 2.0 T. Further investigations with cosputtering, confirmed this assumption that a very small change in composition has a huge influence on the grown films.

To conclude, by varying the sputter Ar pressure, we can change the phase from a SmCo_5 -like to the Sm_2Co_7 -

like phase. We find that the film composition is extremely sensitive to small variation in target composition and the Ar gas pressure used for sputtering. The grown films have good crystal texture and magnetic properties. But, the type of film is not as well defined as might be expected.

V. ACKNOWLEDGMENTS

We thank Roger Wördenweber and Eugen Hollmann for the RBS measurements. Financial support from the European Commission (FP7-ICT-FET No. 225955 STELE) is gratefully acknowledged.

¹T. S. Chin. *J. Magn. Magn. Mater.*, **209**, 75 (2000).

²S. Sawatzki, R. Heller, Ch. Mickel, M. Seifert, L. Schultz, and V. Neu. *J. Appl. Phys.*, **109**, 123922 (2011).

³J. Engelmann, T. Shapoval, S. Haindl, L. Schultz, and B. Holzapfel. *Journal of Physics: Conference Series*, **234**, 012012 (2010).

⁴L. N. Zhang, J. S. Chen, J. Ding, and J. F. Hu. *J. Appl. Phys.*, **103**, 113908 (2008).

⁵A. Singh, V. Neu, R. Tamm, K. Subba Rao, S. Fähler, W. Skrotzki, L. Schultz, and B. Holzapfel. *Appl. Phys. Lett.*, **87**, 072505 (2005).

⁶E. E. Fullerton, C. H. Sowers, J. P. Pearson, S. D. Bader, X. Z. Wu, and D. Lederman. *Appl. Phys. Lett.*, **69**, 2438 (1996).

⁷T. Speliotis and D. Niarchos. *J. Magn. Magn. Mater.*, **290 - 291**, 1195 (2005).

⁸H. Okamoto. *Journal of Phase Equilibria*, **20**, 535 (1999).

⁹B. L. Gordon and M. S. Seehra. *Phys. Rev. B*, **40**, 2348 (1989).

¹⁰J.S. van Wieringen and J.G. Rensen. Influence of lattice imperfections on the paramagnetic resonance of V^{2+} and Cr^{3+} in mgo. In W. Low, editor, *Paramagnetic resonance vol 1*, pages 105–112. Academic Press New York, 1963.

¹¹R. Tamm, K. S. Rao, S. Fhler, V. Neu, A. Singh, C.-G. Oertel, L. Schultz, B. Holzapfel, and W. Skrotzki. *Phys. Status Solidi A*, **207**, 106 (2010).

¹²S. Prucnal, A. Shalimov, M. Ozerov, K. Potzger, and W. Skrupa. *J. Cryst. Growth*, **339**, 70 (2012).

¹³C. H. Chen, S. J. Knutson, Y. Shen, R. A. Wheeler, J. C. Horwath, and P. N. Barnes. *Applied Physics Letters*, **99**, 012504 (2011).